Supplemental Figure 1

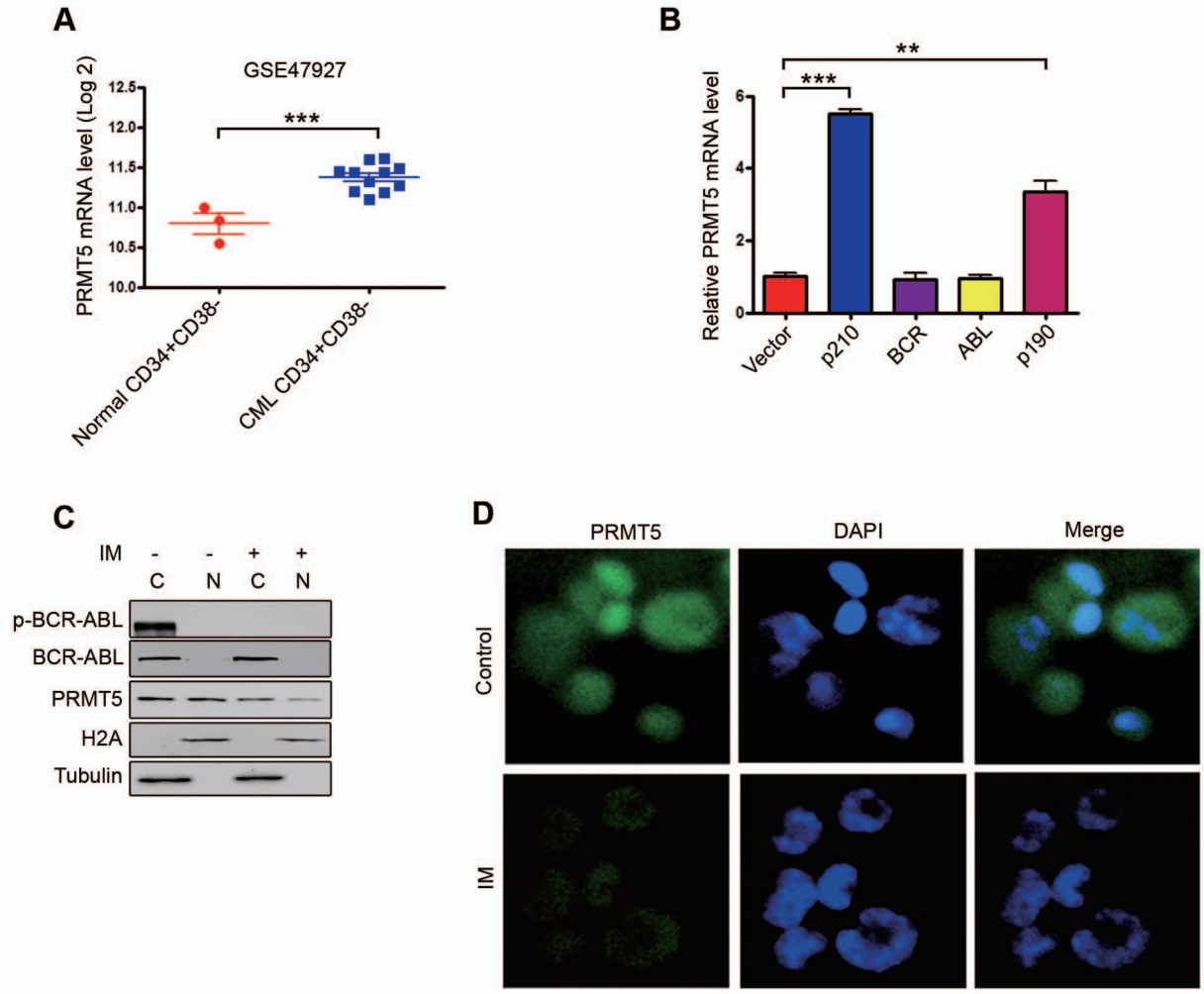

Supplemental Figure 1. BCR-ABL activates PRMT5 expression in human $CD34^+$ cells. Related to Figure 1. (**A**) PRMT5 was overexpressed in CML $CD34^+CD38^-$ cells compared with normal counterparts (GSE47927). *** $P<0.0001$, 2-tailed Student's *t* test. (**B**) Fusion *BCR-ABL* gene activated PRMT5 expression at mRNA level. ** $P<0.01$, *** $P<0.0001$, one-way ANOVA, *post-hoc* intergroup comparisons, Tukey's test. (**C**) Inactivation of BCR-ABL decreased PRMT5 in cytoplasmic and nuclear compartments. Tubulin and H2A were indicators of cytoplasmic and nuclear extractions, respectively. (**D**) K562 cells were treated with IM (1.0 μM) for 24 hr, then underwent immunofluorescent analysis with anti-PRMT5. Nuclei were stained with DAPI.

Supplemental Figure 2

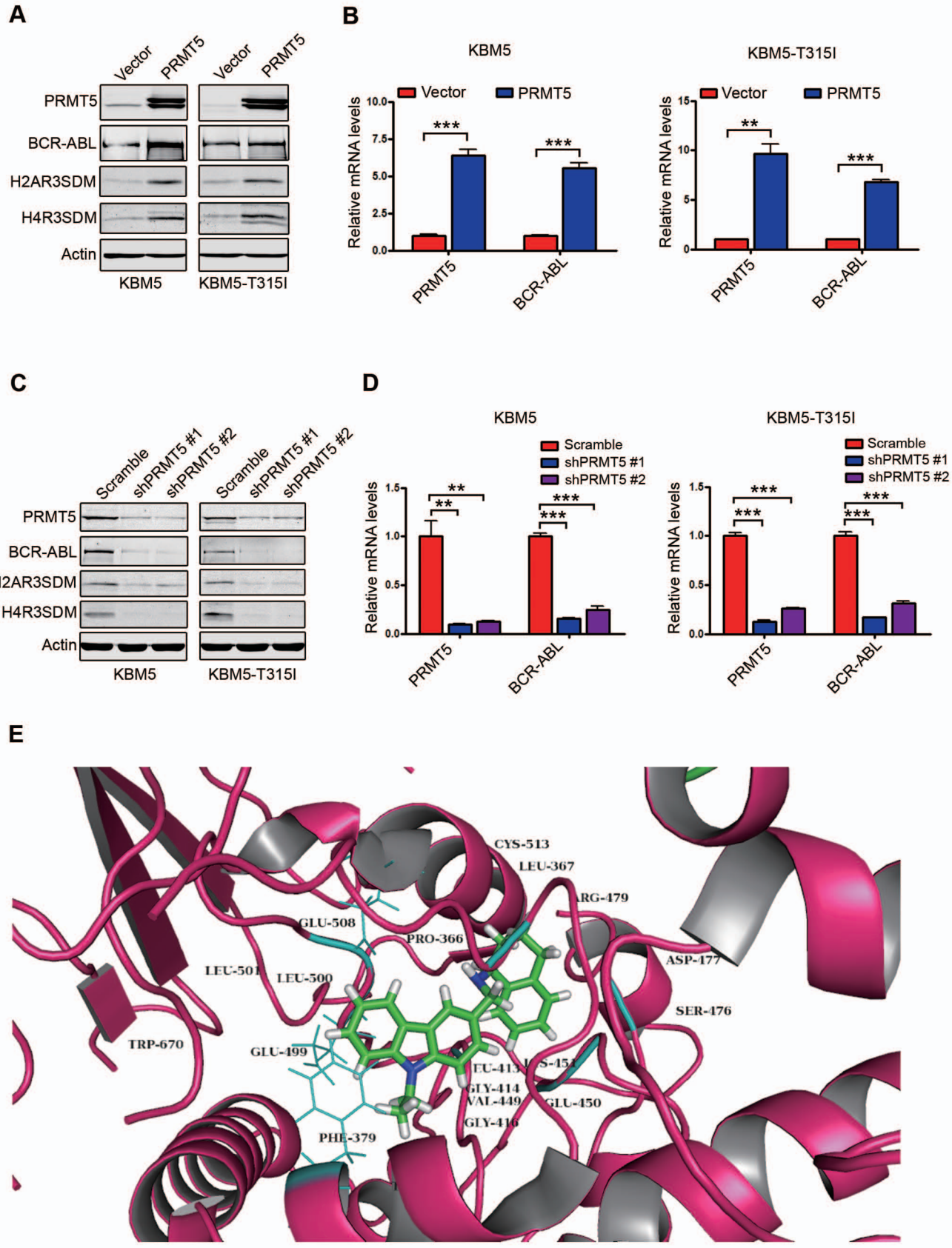

Supplemental Figure 2. PRMT5 positively regulates BCR-ABL expression in CML cells. Related to Figure 2. (**A** and **C**) Fourty-eight hr after KBM5 or KBM5-T315I cells were electrotransfection with pCMV-2B-Flag (vector) or pCMV-2B-Flag-PRMT5 (PRMT5) constructs (A), or 48 hr after two rounds of transduction with control shRNA (Scramble), shPRMT5 #1, or shPRMT5 #2 lentivirus (C), the protein levels of BCR-ABL and PRMT5 and its histone methylation marks (H2AR3SDM and H4R3SDM) were determined by Western blot analysis. (**B** and **D**) Twenty-four hr after KBM5 or KBM5-T315I cells were electrotransfection with pCMV-2B-Flag (vector) or pCMV-2B-Flag-PRMT5 (PRMT5) constructs (B), or 24 hr after two rounds of transduction with control shRNA (Scramble), shPRMT5 #1, or shPRMT5 #2 lentivirus (D), the mRNA levels of *BCR-ABL* and *PRMT5* were determined by qRT-PCR analysis. 2-tailed Student's *t* test was used for **B**; one-way ANOVA, *post-hoc* intergroup comparisons, Tukey's test was performed for **D**. ** $P<0.01$, *** $P<0.0001$. (**E**) Molecular docking studies of PJ-68 and PRMT5. Docked conformation of PJ-68 in the active site of PRMT5 (3 Å surround the binding pocket). The docking between PJ-68 and predicted pocket (in blue cartoons) of PRMT5. The residues labeled in cartoons may form electronic/hydrophobic/aromatic stacking interactions with PJ-68.

Supplemental Figure 3

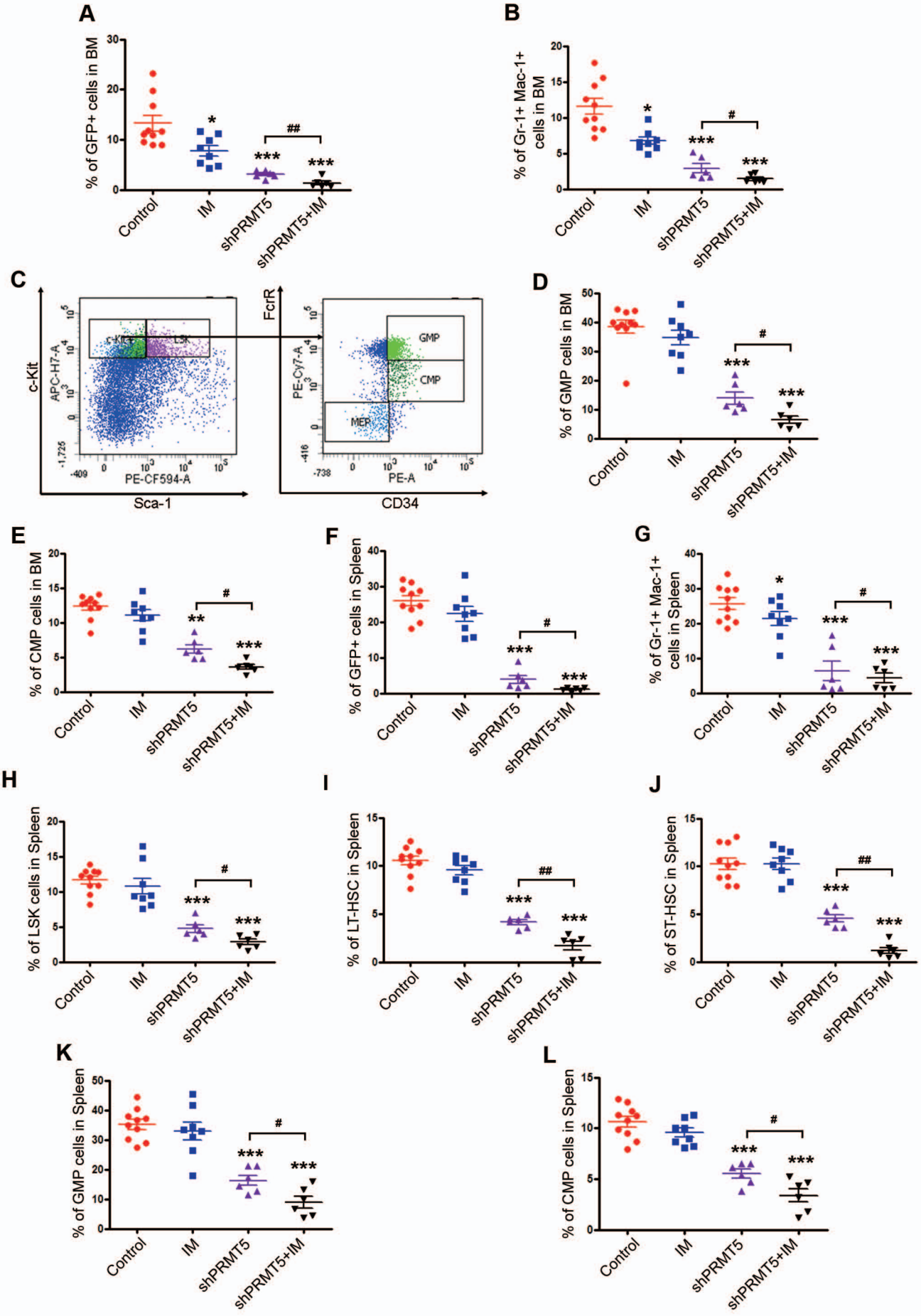

Supplemental Figure 3. *PRMT5* knockdown inhibits LSCs growth in the CML mouse model. Related to Figure 4. (**A**) Percentage of GFP^+ cells (leukemia cells) in BM. (**B**) Percentage of GFP^+ myeloid cells ($Gr\text{-}1^+$ $Mac\text{-}1^+$) in BM. (**C**) Schema for analysis of GMP and CMP in BM cells of CML mice. (**D**) GMP cell proportion in BM. (**E**) CMP cell proportion in BM. (**F**) Percentage of GFP^+ cells (leukemia cells) in the spleens of CML mice. (**G**) Percentage of GFP^+ myeloid cells ($Gr\text{-}1^+$ $Mac\text{-}1^+$) in the spleens of CML mice. (**H-J**) Analysis of LSKs in the spleen cells of CML mice received treatment with shPRMT5 ± IM. Control (n=10), IM (n=8), shPRMT5 (n=6), shPRMT5+IM (n=6). Results for the GFP^+ population in spleen: LSK cells (**H**), LT-HSCs (**I**), and ST-HSCs (**J**). (**K**) GMP cell proportion in spleen. (**L**) CMP cell proportion in spleen. * $P<0.05$, *** $P<0.0001$, compared with control; # $P<0.05$, ## $P<0.01$, shPRMT5 compared with shPRMT5+IM, one-way ANOVA, *post-hoc* intergroup comparisons, Tukey's test.

Supplemental Figure 4

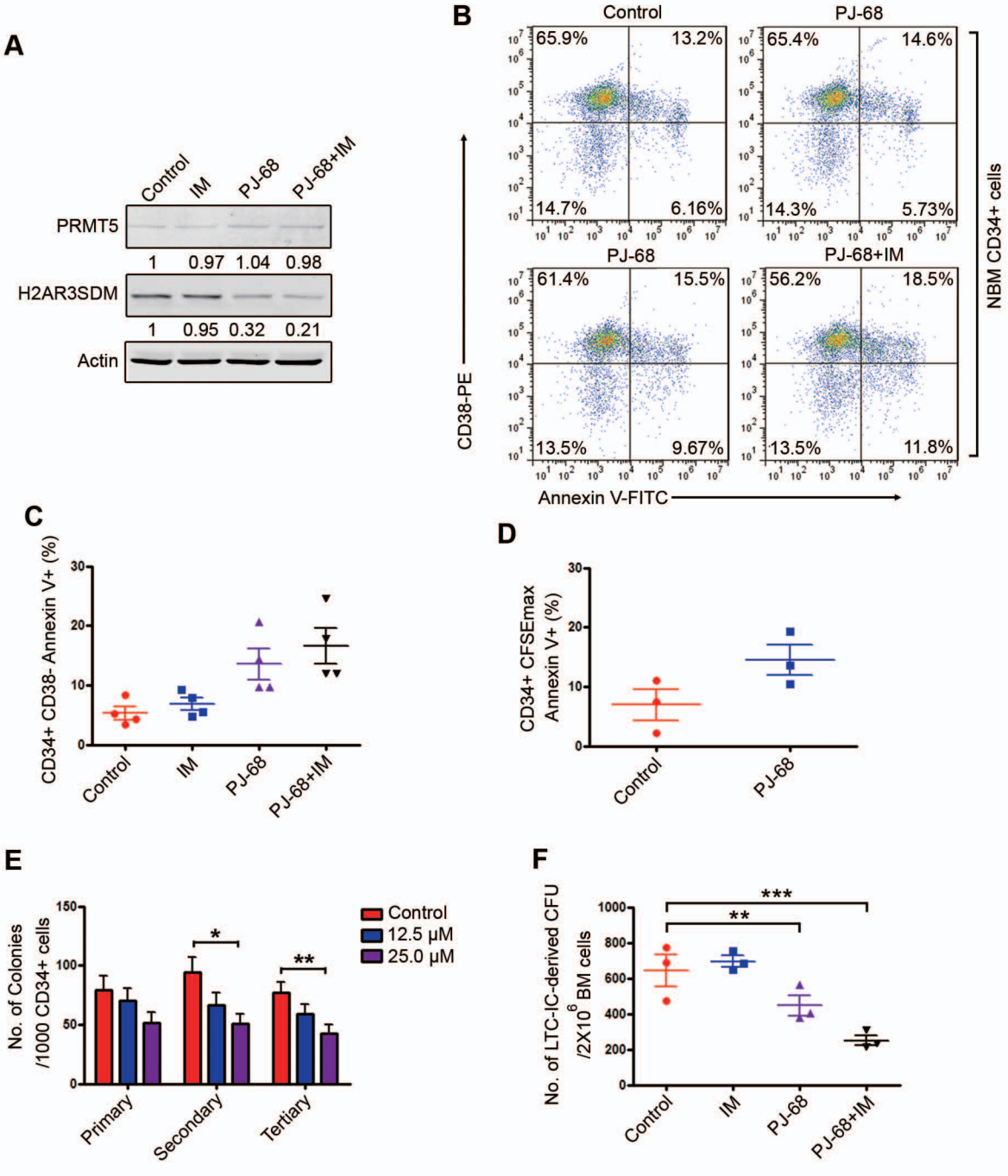

Supplemental Figure 4. Pharmacological inhibition of PRMT5 activity has minimal effect on self-renewal capacity of human NBM CD34$^+$ cells. Related to Figure 5. (**A**) Human NBM CD34$^+$ cells (n=3) were treated with PJ-68 alone or in combination with IM for 24 hr; Western blot analysis of protein levels of PRMT5 and its specific substrate H2AR3SDM. (**B**) Representative flow cytometry plots for apoptosis in human NBM CD34$^+$ cells. (**C**) NBM CD34$^+$ cells (n=4) were treated with PJ-68 alone or with IM (2.5 μM) for 24 hr, apoptosis was analyzed by flow cytometry after staining with Annexin V-FITC and anti-CD38-PE. (**D**) Pharmacological inhibition of PRMT5 activity did not induce apoptosis in quiescent NBM CD34$^+$ cells. Human NBM CD34$^+$ cells (n=3) were labeled with CFSE, then cultured with PJ-68 for 96 hr, apoptotic cells were analyzed by flow cytometry after labeling with Annexin V-PE. (**E**) Pharmacological inhibition of PRMT5 activity exhibited minimal effect on the serial replating capacity of NBM LSCs. Human NBM CD34$^+$ cells (n=3) were treated with concentrations of PJ-68 for 24 hr, washed with PBS and counted; 1,000 cells were plated in methylcellulose medium. Colonies were counted on day 14. The cells were then harvested and 1,000 cells were re-plated for the second and third rounds, and colonies were counted on day 14 after each round. (**F**) Pharmacological inhibition of PRMT5 activity lessened the LTC-IC capacity of NBM LSCs. Human NBM cells (n=3) (2×10^6) were seeded in LTC-IC medium onto irradiated M2-10B4 cells and treated with PJ-68 (25.0 μM) with or without IM (2.5 μM) for 1 week, and cells were cultured for 5 more weeks in LTC-IC medium with weekly half drug-free-medium changes. After 6 weeks, cells were harvested and plated into MethoCult H4435. LTC-IC–derived colonies were counted after 14 days. * P<0.05, ** P<0.01, *** P<0.0001, one-way ANOVA, *post-hoc* intergroup comparisons, Tukey's test.

Supplemental Figure 5

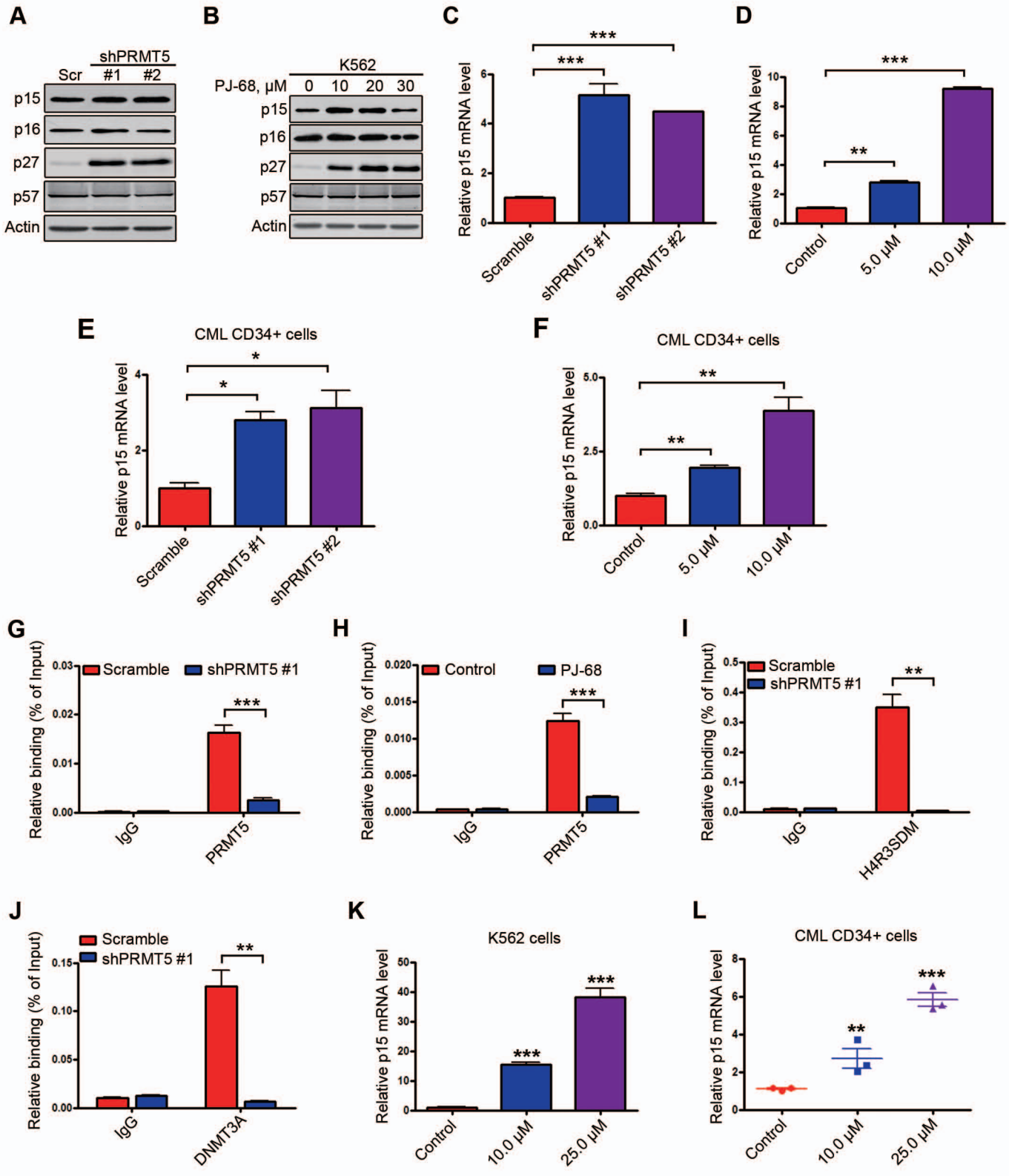

Supplemental Figure 5. PRMT5 modulates the expression of cell cycle regulators in CML CD34$^+$ cells. (**A** and **B**) Knockdown of *PRMT5* or pharmacological inhibition of PRMT5 activity by **s**mall-molecule inhibitor PJ-68 increased p15^{INK4B} and p27^{KIP1} but not p16^{INK4A} and p57^{KIP2} expression. Cell lysates were from stable knockdown K562 cells with Scr (Scramble), shPRMT5 #1 and shPRMT5 #2, or K562 cells incubated with PJ-68 for 24 hr. Western blot analysis of the protein level of p15^{INK4B}, p16^{INK4A}, p27^{KIP1}, and p57^{KIP2}. (**C** and **D**) qRT-PCR analysis of mRNA level of *p15^{INK4B}* in K562 cells transduced with lentiviral shRNA against *PRMT5* (C) or with pharmacological inhibition of PRMT5 activity (D). (**E** and **F**) qRT-PCR analysis of mRNA level of *p15^{INK4B}* in CML CD34$^+$ cells transduced with lentiviral shRNA against *PRMT5* (E) or with pharmacological inhibition of PRMT5 activity (F). (**G** and **H**) *PRMT5* knockdown or inhibition led to loss of recruitment of PRMT5 on the *p15^{INK4B}* promoter. (**I** and **J**) *PRMT5* knockdown inhibited the enrichment of H4R3SDM (I) and DNMT3A (J) at the promoter of *p15^{INK4B}* as detected by ChIP assay in *PRMT5* knockdown K562 cells. Scramble shRNA was a control. (**K** and **L**) DNMT3A inhibition in CML cells upregulated *p15^{INK4B}* expression. K562 cells (K) and CML CD34$^+$ cells (n=3) (L) were treated with the indicated DNMT3A inhibitor for 24 hr, and *p15^{INK4B}* mRNA level was examined by qRT-PCR analysis. 2-tailed Student's *t* test was performed for **G**, **H**, **I** and **J**; one-way ANOVA, *post-hoc* intergroup comparisons, Tukey's test was used for **C**, **D**, **E**, **F**, **K** and **L**. * $P<0.05$, ** $P<0.01$, *** $P<0.0001$.

Supplemental Figure 6

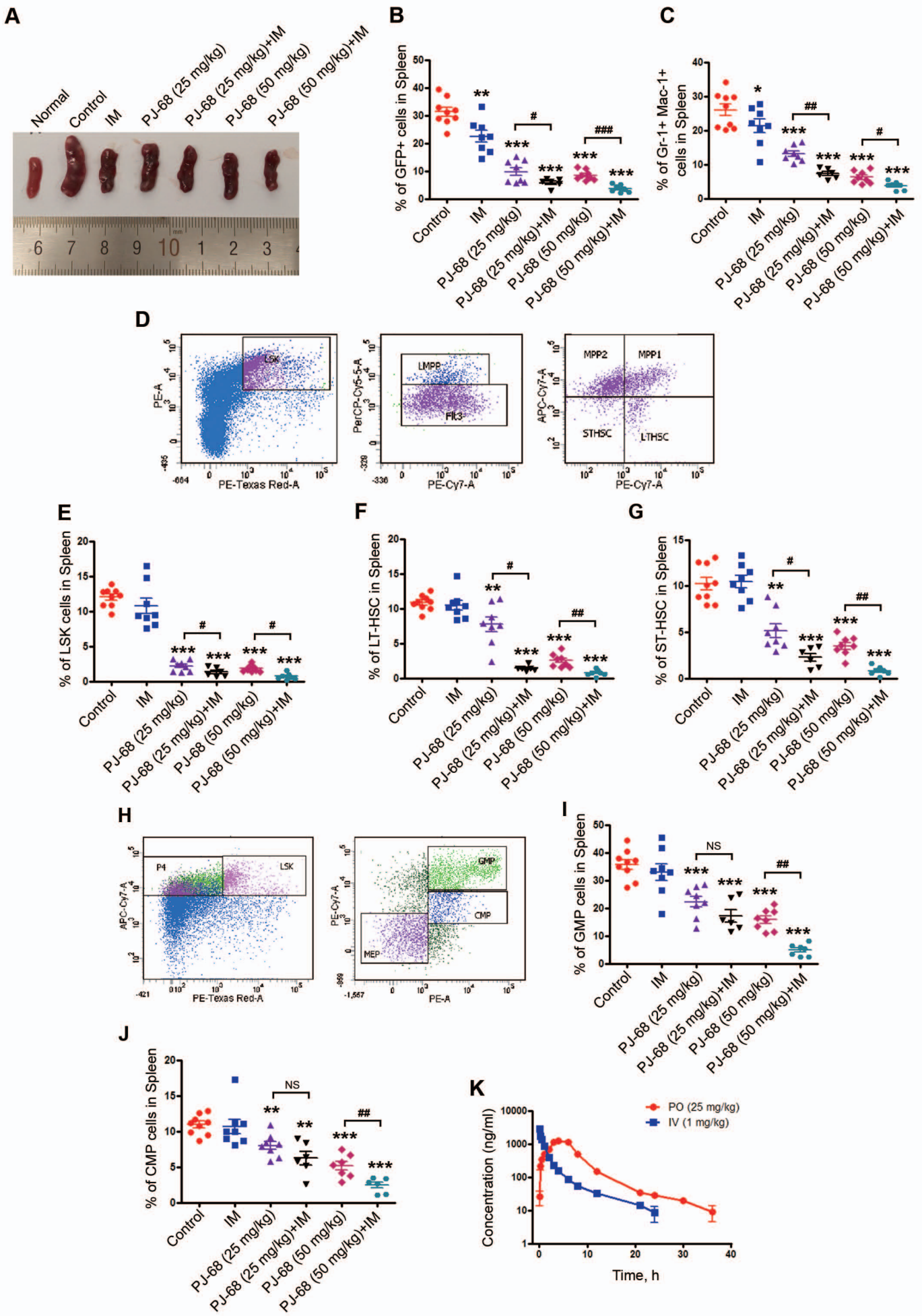

Supplemental Figure 6. Pharmacological inhibition of PRMT5 activity reduces growth of CML stem cells in mice. Related to Figure 6. CML mice were treated with PJ-68 (25 mg/kg/day and 50 mg/kg/day, i.p., respectively) with or without IM (100 mg/kg/day, p.o.) for 2 weeks; mice were enthanized, and bulk leukemia cells and stem/progenitor cells in spleens were analyzed by flow cytometry. (**A**) A representative photograph of spleens from each group. (**B**) GFP^+ (leukemia) cells and (**C**) GFP^+ myeloid cells ($Gr\text{-}1^+$ $Mac\text{-}1^+$) cells in the spleen. (**D**) Schema for analysis of LSKs, LT-HSCs, and ST-HSCs. Results for the GFP^+ population in the spleen were shown: LSK cells (**E**), LT-HSCs (**F**), and ST-HSCs (**G**). (**H**) Schema for analysis of GMP and CMP in spleen cells of CML mice. (**I**) GMP cells and (**J**) CMP cells in the spleen. Control (n=9), IM (n=8), PJ-68 (25 mg/kg) (n=8), PJ-68 (25 mg/kg)+IM (n=6), PJ-68 (50 mg/kg) (n=8), PJ-68 (50 mg/kg)+IM (n=7). * $P<0.05$, ** $P<0.01$, *** $P<0.0001$, compared with control; NS: not significant, # $P<0.05$, ## $P<0.01$, ### $P<0.0001$, PJ-68 compared with PJ-68+IM, one-way ANOVA, *post-hoc* intergroup comparisons, Tukey's test. (**K**) Pharmacokinetics of PJ-68 in SD rats. The plot of PJ-68 plasma concentration *versus* time in SD rats (n=3, each), following single oral gavage administration and intravenous injection was shown.

Supplemental Figure 7

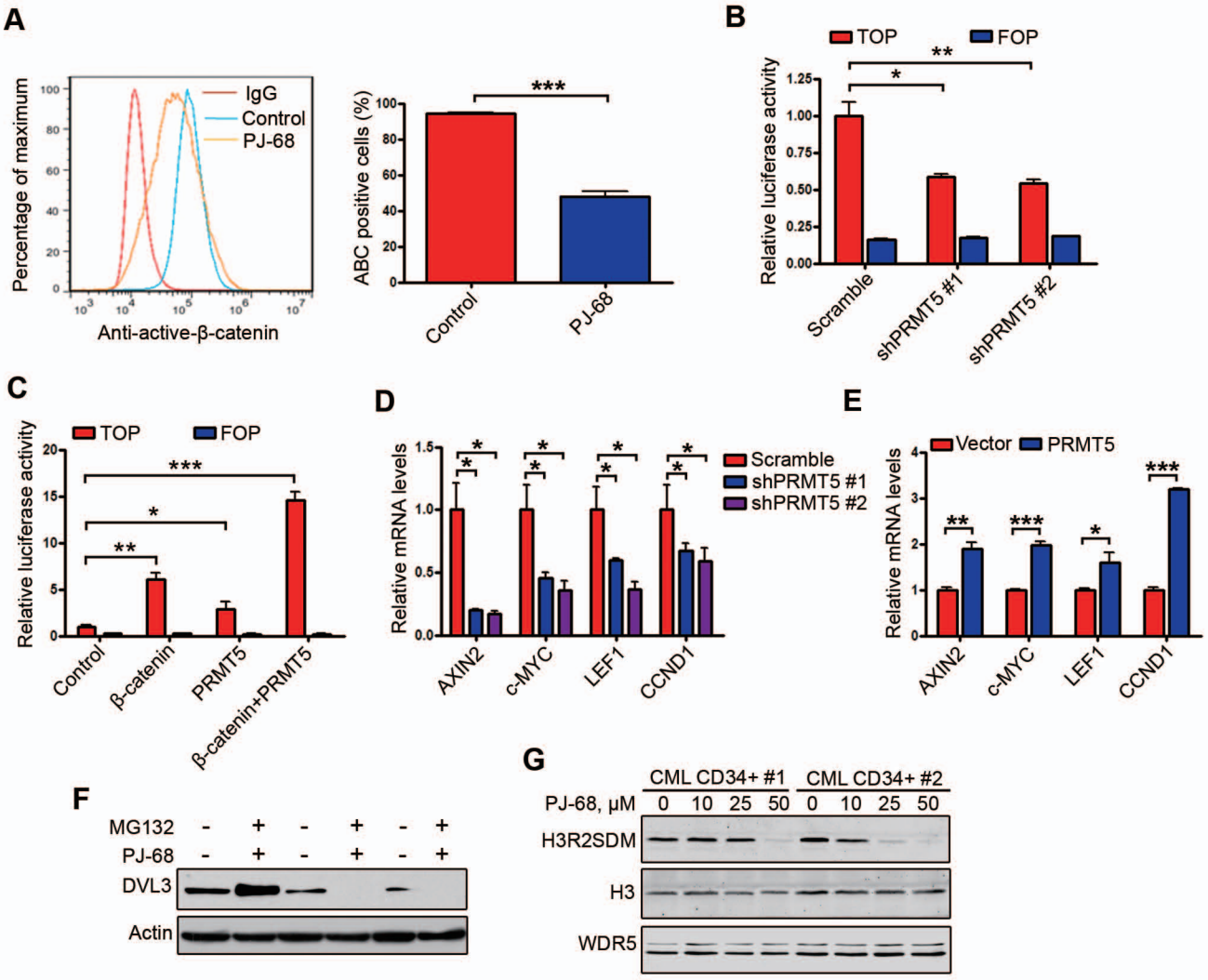

Supplemental Figure 7. PRMT5 activates Wnt/β-catenin signaling through DVL3 in human CML CD34$^+$ cells. Related to Figure 9. (**A**) Pharmacological abrogation of PRMT5 activity decreased active intracellular β-catenin levels in CML cells. Flow cytometry of activated intracellular β-catenin levels in K562 cells after labeled with anti-active-β-catenin (ABC) antibody. A representative flow cytometry plot (left) and bar plots (right) were shown. (**B**) *PRMT5* knockdown elicited TCF4/LEF1-dependent luciferase activity in K562 cells. (**C**) PRMT5 activated TCF/LEF-dependent luciferase activity. (**D**) *PRMT5* knockdown decreased the mRNA levels of Wnt targets genes. (**E**) *PRMT5* overpression increased the mRNA levels of Wnt targets genes. * P<0.05, one-way ANOVA, *post-hoc* intergroup comparisons, Tukey's test. (**F**) Inhibition of ubiquitin-proteasome degradation pathway by MG132 did not rescue PJ-68-mediated inhibition of DVL3. (**G**) *PRMT5* knockdown or inhibition reduced level of H3R2SDM determined by Western blot analysis in CML CD34$^+$ cells (n=2). * P<0.05, ** P<0.01, *** P<0.0001, 2-tailed Student's t test.

Supplemental methods

Molecular docking studies of PJ-68 and PRMT5

Molecular docking was performed using Surflex-Dock (SYBYL®8.1 molecular modeling software) (1). Crystal structure of PRMT5 was retrieved from RCSB Protein Data Bank (PDB entry code: 3UA3). Half of 3UA3 was removed for clarity since it was reported as a homodimer. Molecule was sketched and minimized using Powell optimization in the presence of the Tripos force field with a convergence criterion of 0.001 kcal/mol Å and then assigned with the Gasteiger–Hückel charges. Automatic docking was employed. Other parameters were established by default in software.

Immunoprecipitation

Cells were harvested in Triton/glycerol lysis buffer (1% Triton X-100, 10% glycerol, 150 mM NaCl, 20 mM Tris (pH 7.5), 2 mM EDTA, 1 mM PMSF, 10 μg/ml aprotinin and 10 μg/ml leupeptin, 0.5 μM NaF, and 10 μM β-glycerophosphate) and protein concentration was determined by the BCA assay. After incubating with antibody at 4^{o}C overnight, β-catenin and TCF4 proteins were precipitated using protein A/G agarose (Santa Cruz Biotechnology, Santa Cruz, CA). Precipitated proteins were eluted by 100 mM glycine (pH=3.0), and resolved by SDS-PAGE (2).

NSI mice

We generated the new strain of immunodeficient mice (NOD-scid-IL2Rg−/−) designated NSI by injecting IL2Rg−/− TALENs mRNA pair into the cytoplasm of

pronuclear-stage embryos in the NOD/SCID mice (3). Briefly, female NOD/SCID mice (6-8 weeks of age, Vital River Laboratory Animal Technology Co. Beijing, China) were superovulated by intraperitoneal injection with 5 U of gonadotropin from pregnant mares' serum (PMSG) (cat# G4877-2000IU, Sigma-Aldrich, Shanghai, China) per mouse, followed by injection of 5 U human chorionic gonadotropin (HCG) (cat# CG10-1VL, Sigma-Aldrich, Shanghai, China) 48 hr later. After setting up mating pairs consisting of one superovulated female and one male per cage for overnight, the mating female mice were checked for the presence of vaginal plugs next morning. TALEN-encoding mRNA targeted to *Il2rg* (25 ng/μl) was then microinjected into the cytoplasm of pronuclear-stage embryos. Surviving embryos were surgically implanted into the oviducts of surrogate ICR female mice (Guangzhou Institutes of Biomedicine and Health, Chinese Academy of Sciences, Guangzhou, China). The offsprings were analyzed for knocking-out of *Il2rg* gene. All mice were bred and maintained in specific pathogen-free (SPF)-grade cages and provided with autoclaved food and water. The phenotypes of NSI mice exhibited deficiency of T, B, and NK cells in the peripheral blood, spleen, and bone marrow, which were similar with the phenotypes of NSG mice.

Site-directed mutagenesis

A catalytically dead PRMT5 mutant construct pCMV-2B-Flag-PRMT5 (R368A) was created using the TaKaRa MutanBEST Kit (Takara Biomedical Technology, Beijing, China) according to the manufacturer’s instructions. Briefly, two

complimentary oligonucleotides containing the desired mutation were synthesized, PCR reactions were performed. The blunting kination enzyme mix was added to PCR products. The transformation was performed using the DH5α competent cells. The mutated PRMT5 construct was used for transfection. The mutation was performed using the following primers: Forward, 5'-CAGGAgccGGACCCCTGGTGAACGCTTC-3', Reverse, 5'-CTCCCAGCACCATCAGTACCT -3'.

Lentiviral transduction of K562 cells

K562 cells (5×10^5 cells/ml) were infected by spinoculation (1,500 g, 90 min, 32^{o}C) with virus-containing supernatants two rounds in the presence of 8 μg/ml polybrene (Sigma-Aldrich, Shanghai, China). Stable cell lines were established after 1 μg/ml puromycin selection for 3 weeks.

Establishment of K562 cells stably expressing PRMT5

K562 cells were electrotransfected with pCMV-2B-Flag-PRMT5 construct, then treated with G418 (400 μg/ml) for 2 weeks; single clones (#16 and #19) stably expressing PRMT5 were selected by limiting dilution.

Generating the BCR-ABL-promoter luciferase construct

A 1,000-bp fragment 5' upstream from BCR-ABL gene transcription start was amplified by PCR with BCR-ABL promoter primers, then subjected to double

digestion with Xho Ⅰ and Hind Ⅲ restriction enzymes and ligased into pGL3-Basic firefly luciferase reporter vector (Promega, Shanghai, China) to obtain the BCR-ABL-promoter-pGL3 reporter construct. Sequence of the BCR-ABL-promoter-pGL3 construct was confirmed by double restriction digestion analysis and sequencing. The PCR product was cloned into the pGL3-basic vector and the insert was verified by sequencing.

MiR-203 expression assay

Human miR-203 and internal control U6 snRNA were purchased from Life Technologies (Shanghai, China), miR-203 gene was amplified by qPCR according to the manufacturer's instructions (4).

In vitro histone methyltransferase activity assay

The recombinant human PRMTs and substrate were obtained from BPS Bioscience (San Diego, CA). The PRMT enzymatic reactions were conducted in duplicate at room temperature for 60 min in 50 μl containing methyltransferase assay buffer, S-adenosylmethionine, enzyme, and compound PJ-68. The reactions were carried out in a substrate pre-coated plate. The final DMSO concentration is 1%. After enzymatic reactions, the reaction mixtures were discarded and the wells was washed three times with TBST buffer, and slowly shaken with blocking buffer for 10 min. Then 100 μl of diluted primary antibody was added. The plate was slowly shaken for 60 min, washed three times, and shaken with blocking buffer for 10 min.

Then 100 µl of diluted secondary antibody was added. The plate was slowly shaken for 30 min, washed three times, and shaken with blocking buffer for 10 min. A mixture of the HRP chemiluminescent substrates was freshly prepared and added. The luminescence of the samples was measured in a microplate reader immediately. The luminescence data were analyzed and compared. In the absence of the compound, the intensity (Ce) was defined as 100% activity. In the absence of enzyme, the intensity (C0) was defined as 0% activity. The percent activity in the presence of compound was calculated according to the following equation: % activity = (C-C0)/(Ce-C0), where C= the luminescence in the presence of the compound. The concentration for 50% inhibition of enzymatic activity (IC_{50}) was calculated with normalized dose−response fit using GraphPad 5.0 software.

Pharmacokinetic study

Male Sprague–Dawley (SD) rats (n=6) (Vital River Laboratory Animal Technology Co. Beijing, China), weight 200-250 g, were randomly separated in two groups. PJ-68 were dissolved in DMSO (10%), Cremaphor EL (18%) and 5% dextrose (72%). The rats were given PJ-68 either by intravenous infusion (1.0 mg/kg) or oral gavage (25 mg/kg) for pharmacokinetic study. Peripheral blood samples (approximately 0.2 ml/sample) were collected from each animal via the jugular vein at 5, 15, 30 min, 1, 2, 3, 4, 6, 8, 12, 21, 24, 30, 36, 48, 60 and 72 hr after given PJ-68. Blood samples were centrifuged at 8,000 rpm for 6 min, the plasma was collected and stored at -80 °C until analysis. The plasma samples were analyzed by LC-MS/MS (liquid chromatography coupled with tandem mass spectrometry), 450 µl internal

standard solution (5 μg/ml, acetonitrile) was added to 50 μl plasma samples to precipitate proteins. After centrifugation at 14,000 rpm, 4 °C for 5 min, the supernatant (200 μl) was introduced into the LC-MS/MS system. Detection was performed by using API 4000 mass spectrometer (Applied Biosystems) with TurboIonSpray source interface. The data was analyzed by Analyst software (Applied Biosystems, Foster City, CA) (5).

References

1. Jin Y, et al. Ponatinib efficiently kills imatinib-resistant chronic eosinophilic leukemia cells harboring gatekeeper mutant T674I FIP1L1-PDGFRalpha: roles of Mcl-1 and beta-catenin. *Mol Cancer.* 2014;13:17.
2. Han B, et al. FOXC1 Activates Smoothened-Independent Hedgehog Signaling in Basal-like Breast Cancer. *Cell Rep.* 2015;13(5):1046-58.
3. Ye W, et al. Quantitative evaluation of the immunodeficiency of a mouse strain by tumor engraftments. *J Hematol Oncol.* 2015;8:59.
4. Song L, et al. TGF-beta induces miR-182 to sustain NF-kappaB activation in glioma subsets. *The Journal of clinical investigation.* 2012;122(10):3563-78.
5. Zhang Z, et al. GZD856, a novel potent PDGFRalpha/beta inhibitor, suppresses the growth and migration of lung cancer cells in vitro and in vivo. *Cancer Lett.* 2016;375(1):172-8.

Supplemental Table 1. Characteristics of patients with chronic myelogenous leukemia

Patient No.	Gender/ Age (yr)	Disease stage	Sample	Date of diagnosis	Prior therapy	Leukocyte count (10^9/L)	Blast (%)	BCR-ABL–positive
1	M/39	CP	PB	1/2014	Initial	558.71	8%	+
2	M/28	CP	BM	1/2014	Initial	84.54	7%	+
3	F/10	CP	BM	1/2014	Initial	670	5%	+
4	F/25	CP	BM	2/2014	Initial	339.95	13%	+
5	F/23	CP	PB	3/2014	Initial	188.8	4%	+
6	M/55	AP	BM	2/2014	Initial	152.8	5%	+
7	M/23	CP	BM	10/2014	Initial	121.5	3%	+
8	M/22	AP	BM	4/2014	Initial	216.5	2.5%	+
9	M/44	CP	PB	4/2014	Initial	338.95	5%	+
10	F/51	CP	PB	4/2014	Initial	241.39	7%	+
11	M/23	CP	BM	4/2014	Initial	184.30	1%	+
12	M/49	CP	BM	5/2014	Initial	67.62	1%	+
13	M/41	CP	BM	2/2013	Imatinib	213.6	ND	+
14	F/30	CP	BM	8/2014	Initial	361.08	3%	+
15	M/31	BP	PB	8/2014	Initial	809.49	54%	+ (T315I mutation)
16	F/38	CP	PB	9/2014	Initial	312.37	3.65%	+
17	F/18	AP	BM	9/2014	Initial	49.46	9%	+
18	M/43	CP	BM	9/2014	Initial	310.39	8.5%	+
19	M/40	CP	BM	10/2014	Initial	483.85	2%	+
20	M/31	BP	PB	1/2016	Imatinib resistance	41	91%	+
21	F/42	BP	BM	1/2016	Initial	389	ND	+
22	M/39	BP	PB	12/2015	Initial	229.5	ND	+

CP: chronic phase; AP: accelerated phase; BP: blast crisis phase; PB: peripheral blood;

BM: bone marrow; ND: not detected.

Supplemental Table 2. Pharmacokinetics (mean ± standard deviation) of PJ-68 in Sprague-Dawley (SD) rats.

PJ-68	$T_{1/2}$ (hr)	T_{max} (hr)	C_{max} (ng/ml)	$AUC_{(0-t)}$ (ng/ml*hr)	$AUC_{(0-\infty)}$ (ng/ml*hr)
IV 1mg/kg	7.76 ± 1.15	0.08 ± 0.00	2788.5 ± 109.7	3496.3 ± 129.0	3639.9 ± 145.5
PO 25 mg/kg	7.75 ± 3.49	3.67 ± 0.58	1264.4 ± 28.4	9416.1 ± 32.7	9575.7 ± 87.6

Abbreviations: $T_{1/2,}$ half life; AUC, area under the plasma concentration–time curve; Tmax, time to reach peak concentration; Cmax, peak concentration.

Supplemental Table 3. Primers for qRT-PCR

Genes	Sense primer	Antisense primer
PRMT5	5'-CCTGTGGAGGTGAACACAGT-3'	5'-AGAGGATGGGAAACCATGAG-3'
BCR-ABL	5'-TCCACTCAGCCACTGGATTTAA-3'	5'-TGAGGCTCAAAGTCAGATGCTACT-3'
DVL3	5'-CGCCTAGACGACTTCCACTT-3'	5'-CCGATGAAAGCATTAGGGAT-3'
AXIN2	5'-TCAAGTGCAAACTTTCGCCAACC-3'	5'-TAGCCAGAACCTATGTGATAAGG-3'
c-MYC	5'-CAGCGACTCTGAGGAGGAAC-3'	5'-TCGGTTGTTGCTGATCTGTC-3'
LEF1	5'-CGAATGTCGTTGCTGAGTGT-3'	5'-GCTGTCTTTCTTTCCGTGCT-3'
CCND1	5'-GCTGTGCATCTACACCGACA-3'	5'-CCACTTGAGCTTGTTCACCA-3'
$p15^{INK4B}$	5'-GAATGCGCGAGGAGAACAAG-3'	5'-CATCATCATGACCTGGATCGC-3'
18S	5'-AAACGGCTACCACATCCAAG-3'	5'-CCTCCAATGGATCCTCGTTA-3'

Primers for ChIP

Primer	Sequence
PRMT5-promoter-1 Sense	5'-GGGTCTTCCAGCTTTCCTGC-3'
PRMT5-promoter-1 Antisense	5'-TCACTGAATGGCTAGGCACAA-3'
PRMT5-promoter-2 Sense	5'-GAAATTGGGGCTGACCTCCC-3'
PRMT5-promoter-2 Antisense	5'-GAACCCTCCTACCACTCACC-3'
BCR-ABL-promoter Sense	5'-GAGCCAAGTGTTCCTGTTCCA-3'
BCR-ABL-promoter Antisense	5'-CCCGTCCCTGTGCCTTTT-3'
miR-203-promoter Sense	5'-ATCAGTCGCGGGACCTATGG-3'
miR-203-promoter Antisense	5'-GGCGCCTTTTATGCGGC-3'
$p15^{INK4B}$-promoter Sense	5'-AGGGCAGTGGTGAACATTCC-3'
$p15^{INK4B}$-promoter Antisense	5'-AAGCCTGCCCAAAGATGCTA-3'
DVL3-promoter Sense	5'-ACTACCTTGCAACTGGACGC-3'
DVL3-promoter Antisense	5'-TCAACATGGCCCTTCAGTGT-3'

Supplemental Table 4. Information of secondary antibodies for Western blot analysis.

Antibody	Source	Catalog number
Goat-Anti-Mouse 800CW	LICOR Corporate (Lincoln, NE)	926-32210
Goat-Anti-Rabbit 800CW	LICOR Corporate	926-32211
Goat-Anti-Mouse 680RD	LICOR Corporate	926-68070
Goat-Anti-Rabbit 680RD	LICOR Corporate	926-68071
HRP-anti-Mouse	Thermo Fisher Scientific (Waltham, MA)	31437
HRP-anti-Rabbit	Thermo Fisher Scientific	31463

Supplemental Table 4. Information of antibodies for CML mice model.

Antibody (Clone)	Source	Catalog number
Lin-APC	BD Biosciences	51-9003632
c-Kit-PE (2B8)	eBioscience (San Diego, CA)	12-1171-8
c-Kit-APC-H7 (2B8)	BD Biosciences	560185
Sca-1-PE-CF594 (D7)	BD Biosciences	562730
CD135-PE-cy5 (A2F10)	eBioscience	15-1351-82
CD150-PE-cy7 (mShad150)	eBioscience	25-1502-82
CD48-APC-cy7 (HM48-1)	BD Biosciences	561242
CD34-PE (RAM34)	BD Biosciences	551387
CD16/32-PE-Cy7 (93)	eBioscience	25-0161-82
Mac-1(CD11b)-PE (M1/70)	BD Biosciences	553311
Gr-1-APC (RB6-8C5)	BD Biosciences	553129

Information of antibodies for NSI mice.

Antibody (Clone)	Source	Catalog number
CD45-FITC (HI30)	eBioscience	11-0459-42
CD34-FITC (4H11)	eBioscience	11-0349-42
CD33-PE-Cy7 (P67.6)	BD Biosciences	333952
CD11B-PE (ICRF44)	BD Biosciences	555388
CD19-APC (HIB19)	BD Biosciences	555415
CD14-PerCP-Cy5.5 (MφP9)	BD Biosciences	562692
CD3-Alexa Fluor 700 (UCHT1)	BD Biosciences	557943

Supplemental Figure 8

Figure 1B

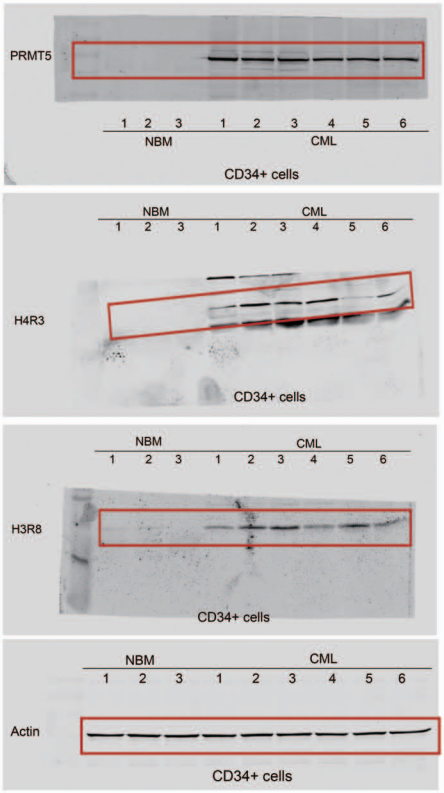

Figure 1E

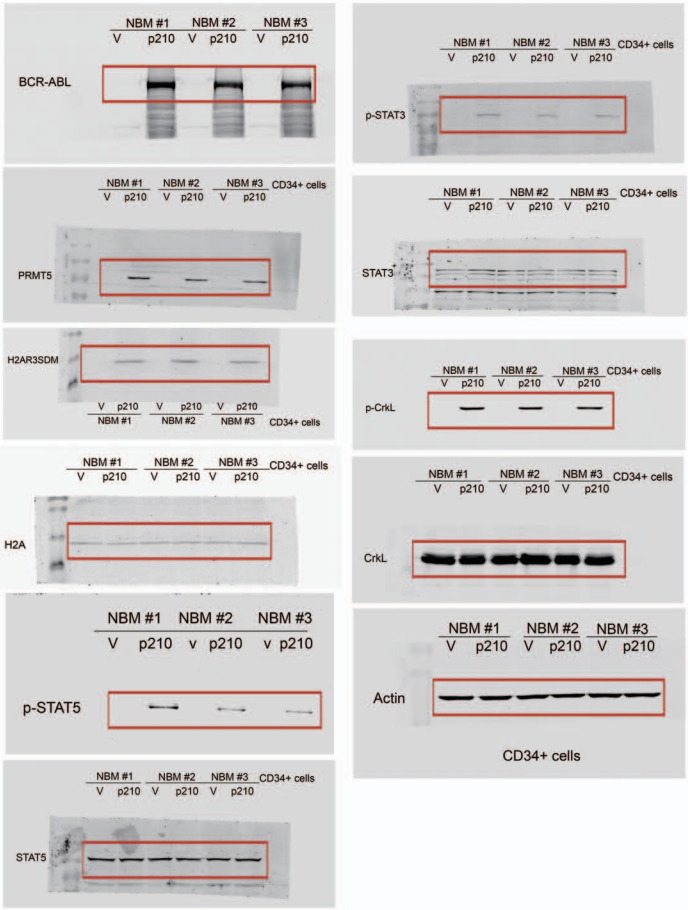

Figure 1F

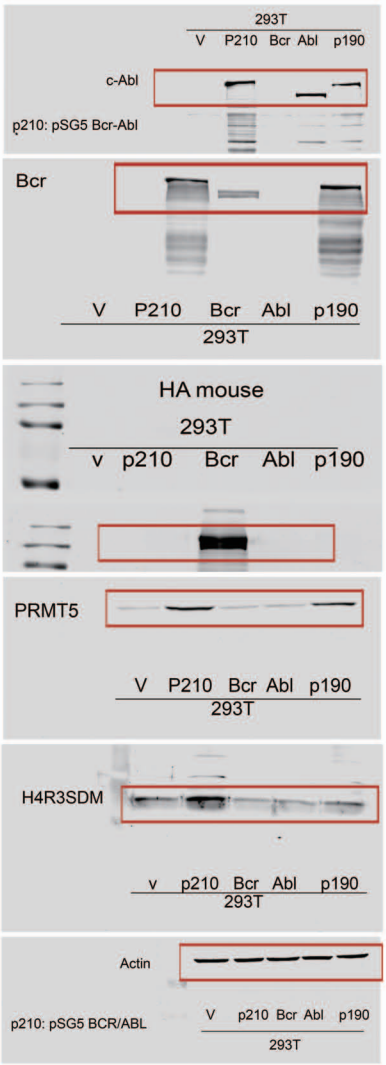

Figure 1G

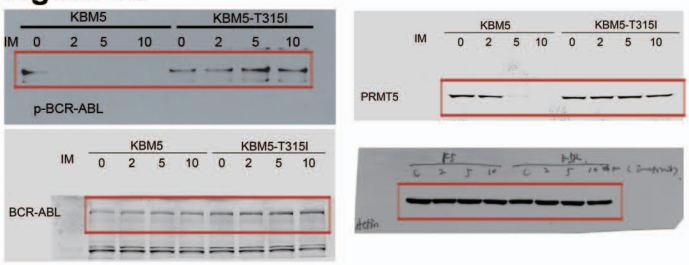

Figure 1H

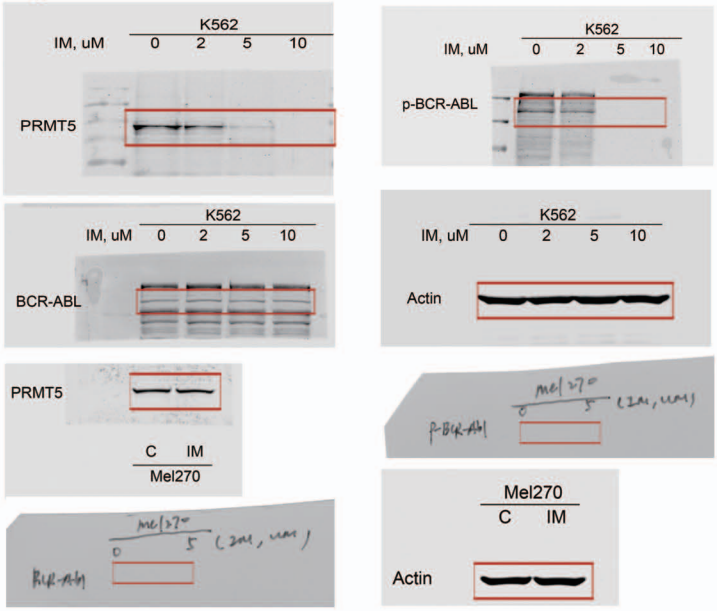

Supplemental Figure 8: Full unedited gel for Figure 1B E F G H, red boxes indicate images shown in the corresponding Figures.

Supplemental Figure 8 Continued

Figure 1J

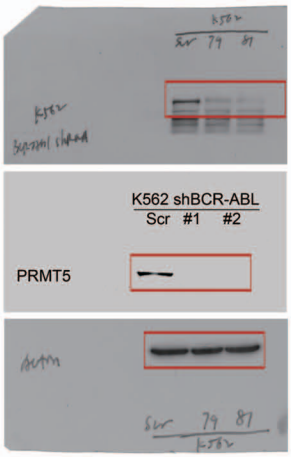

Figure 1K

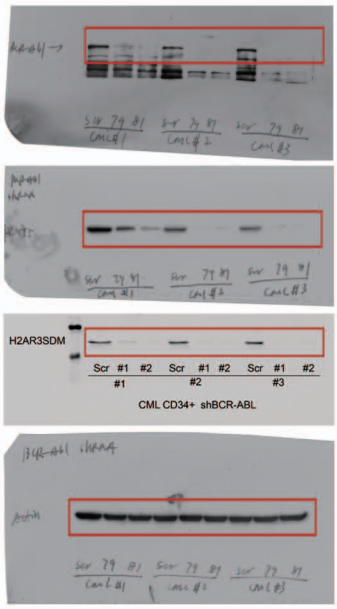

Figure 1N

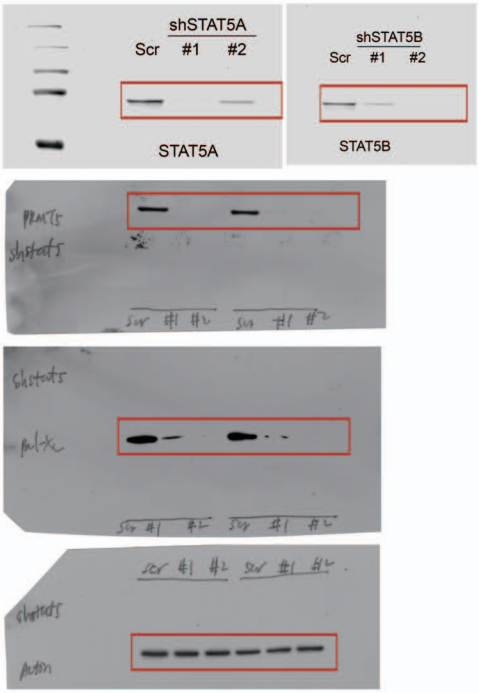

Supplemental Figure 8 continued: Full unedited gel for Figure 1 J K N, red boxes indicate images shown in the corresponding Figures.

Supplemental Figure 9

Figure 2A

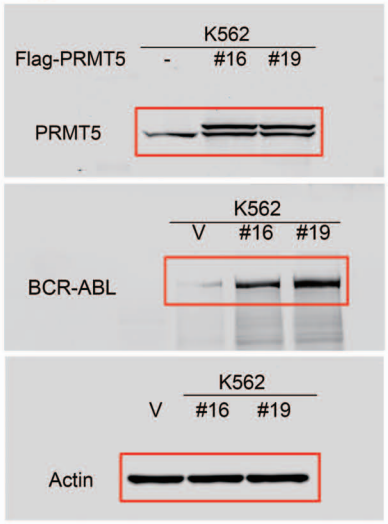

Figure 2B

Figure 2E

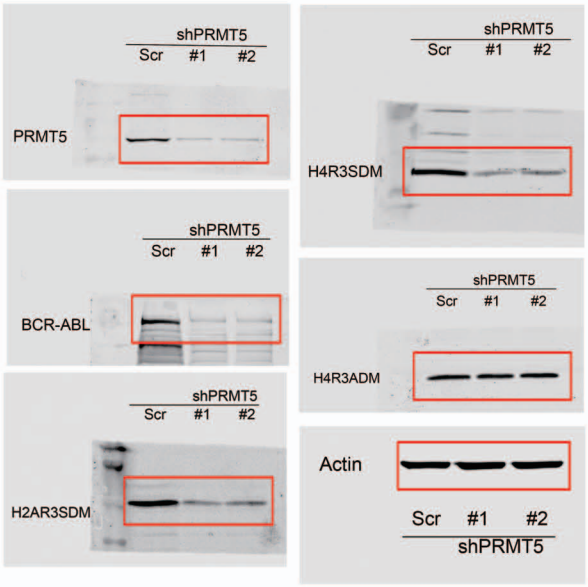

Figure 2I

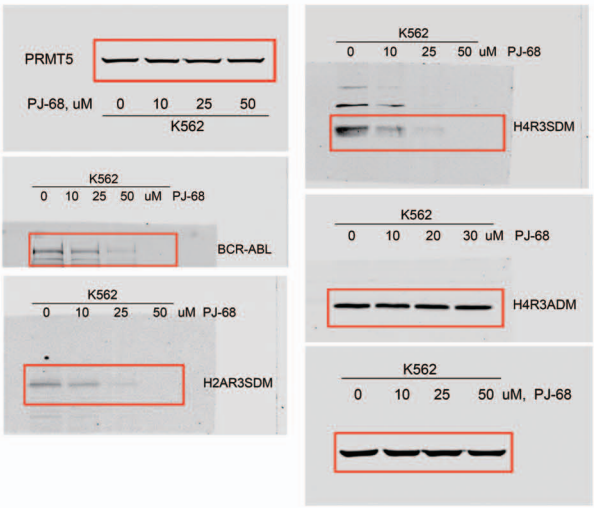

Figure 2L

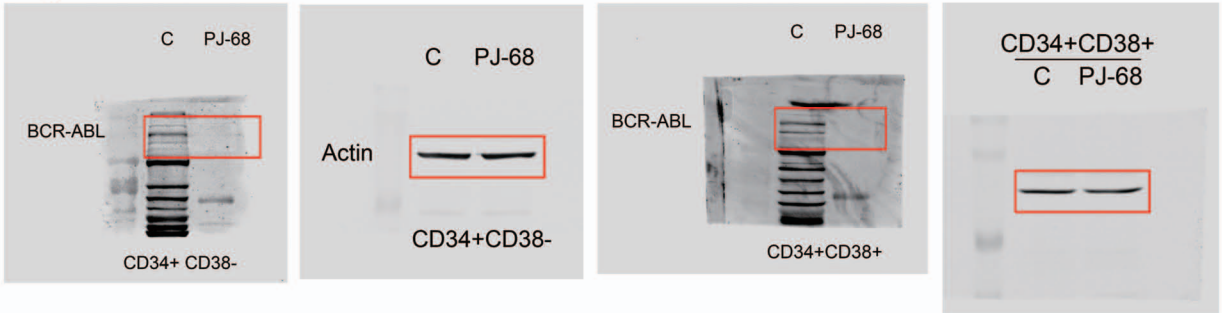

Supplemental Figure 9: Full unedited gel for Figure 2 A B E I L, red boxes indicate images shown in the corresponding Figures.

Supplemental Figure 10

Figure 3A

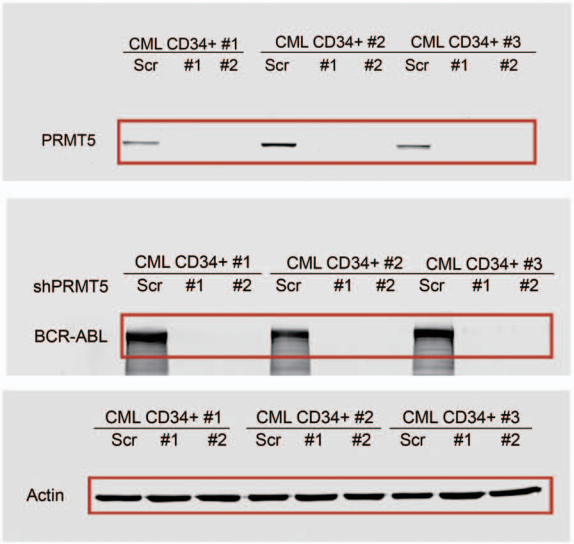

Figure 3B

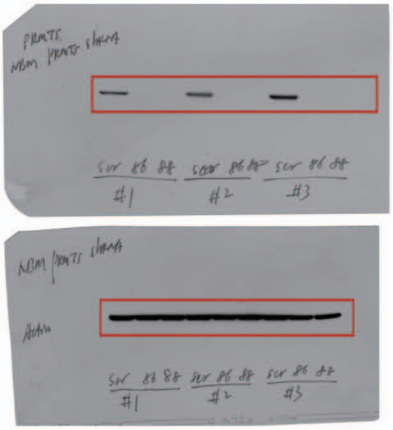

Supplemental Figure 10: Full unedited gel for Figure 3A and 3B, red boxes indicate images shown in the corresponding Figures.

Supplemental Figure 11

Figure 4B

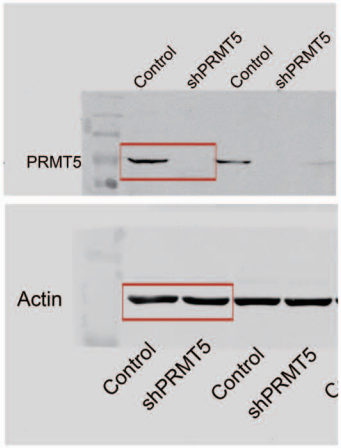

Figure 5A and Supplemental 4A

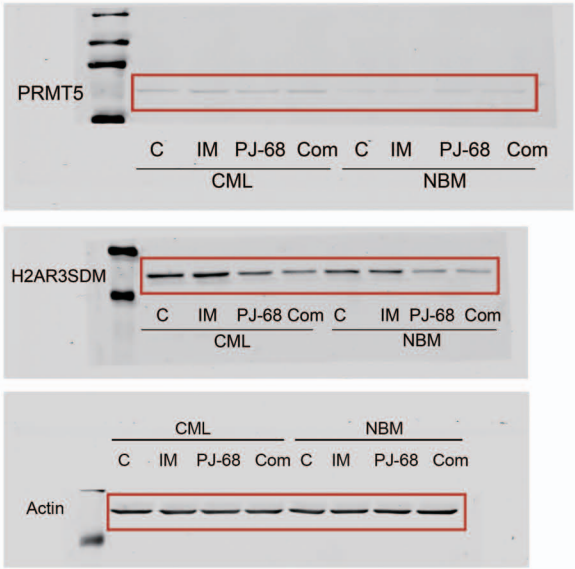

Supplemental Figure 11: Full unedited gel for Figure 4B, Figure 5A and Supplemental 4A, red boxes indicate images shown in the corresponding Figures.

Supplemental Figure 12

Figure 9A and 9B

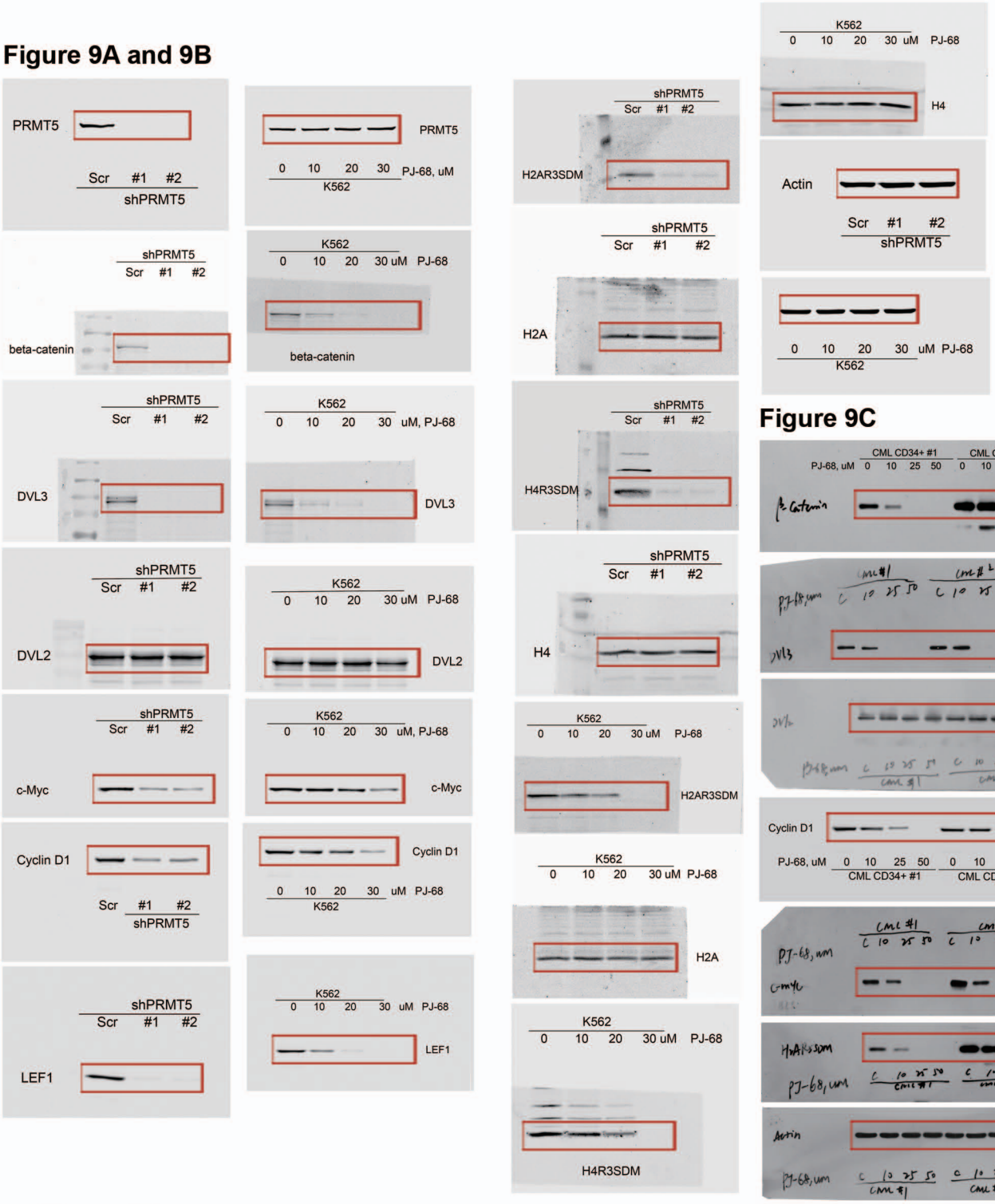

Figure 9C

Figure 9D

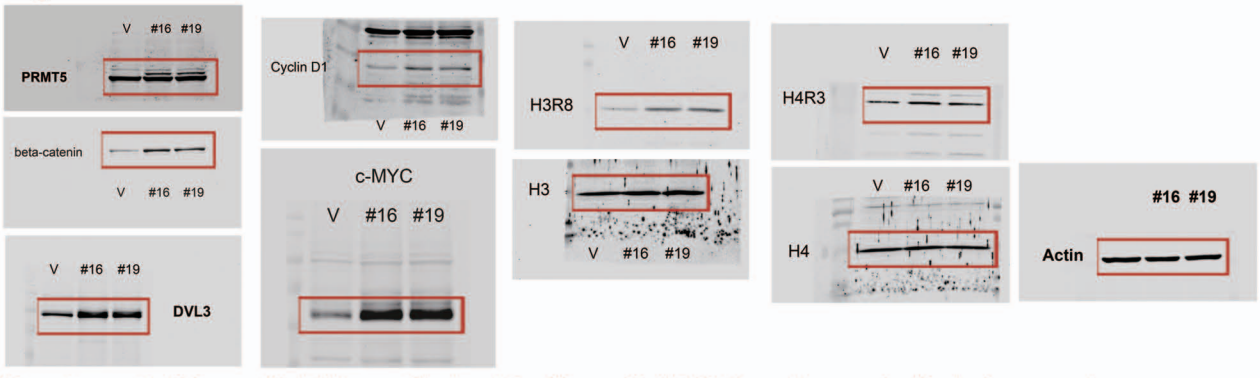

Supplemental Figure 12: Full unedited gel for Figure 9 A B C D, red boxes indicate images shown in the corresponding Figures.

Supplemental Figure 12 Continued

Figure 9G

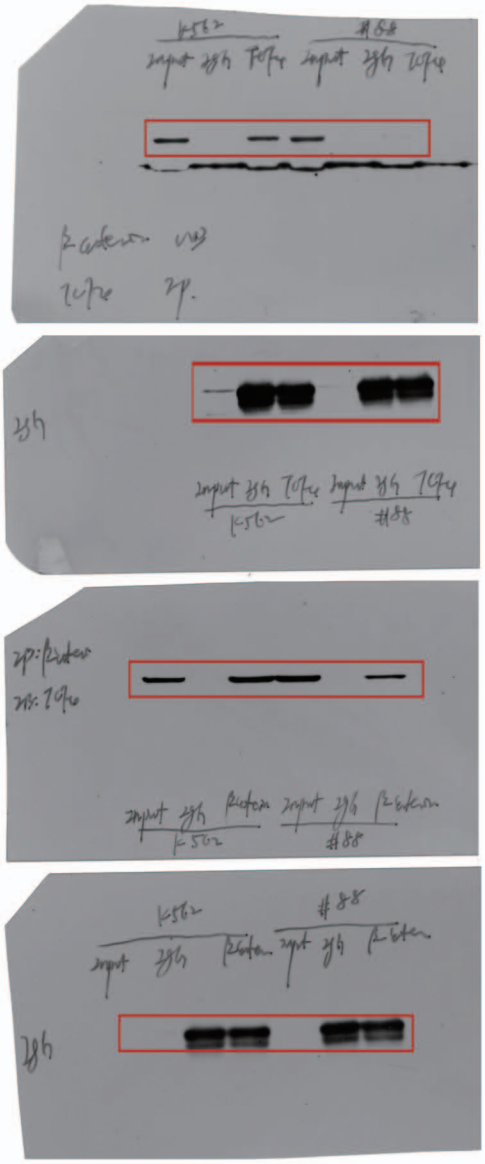

Figure 9J

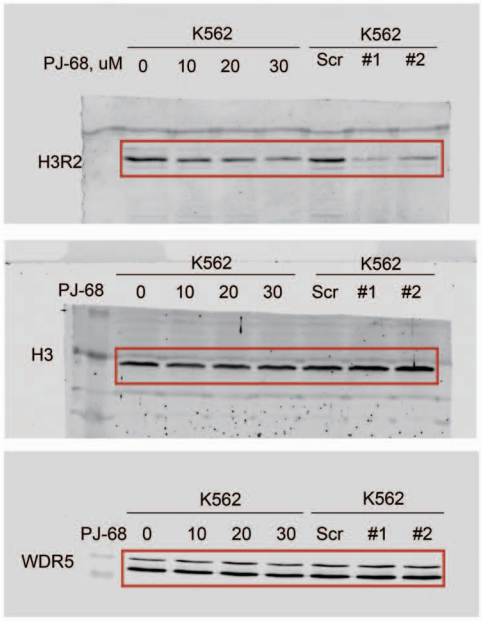

Supplemental Figure 12 continued: Full unedited gel for Figure 9G and 9J, red boxes indicate images shown in the corresponding Figures.

Supplemental Figure 13

Supplemental Figure 1C

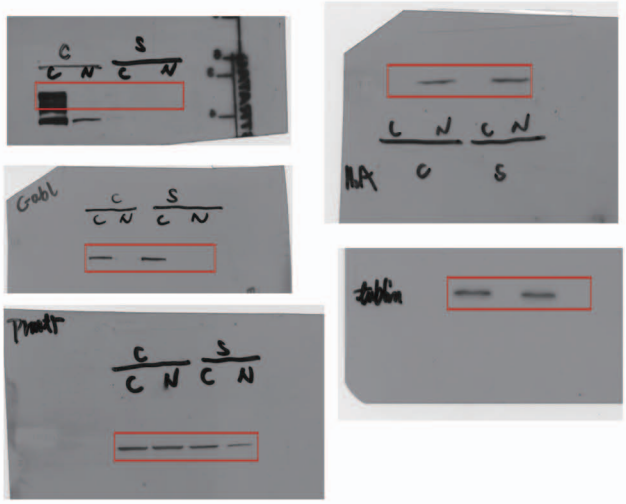

Supplemental Figure 13: Full unedited gel for Supplemental Figure 1C, red boxes indicate images shown in the corresponding Figures.

Supplemental Figure 14

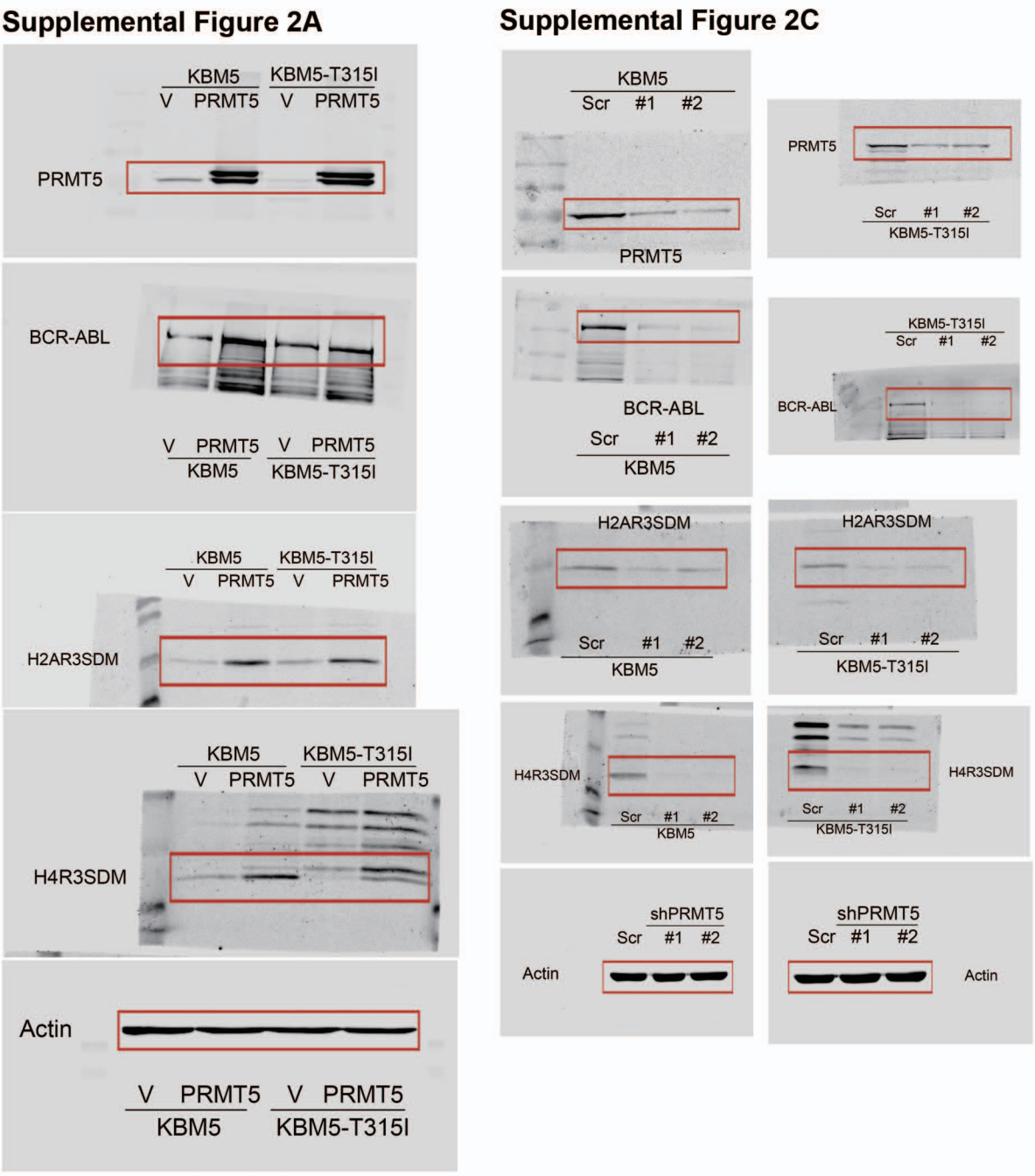

Supplemental Figure 14: Full unedited gel for Supplemental Figure 2A and 2C, red boxes indicate images shown in the corresponding Figures.

Supplemental Figure 15

Supplemental Figure 5A and 5B

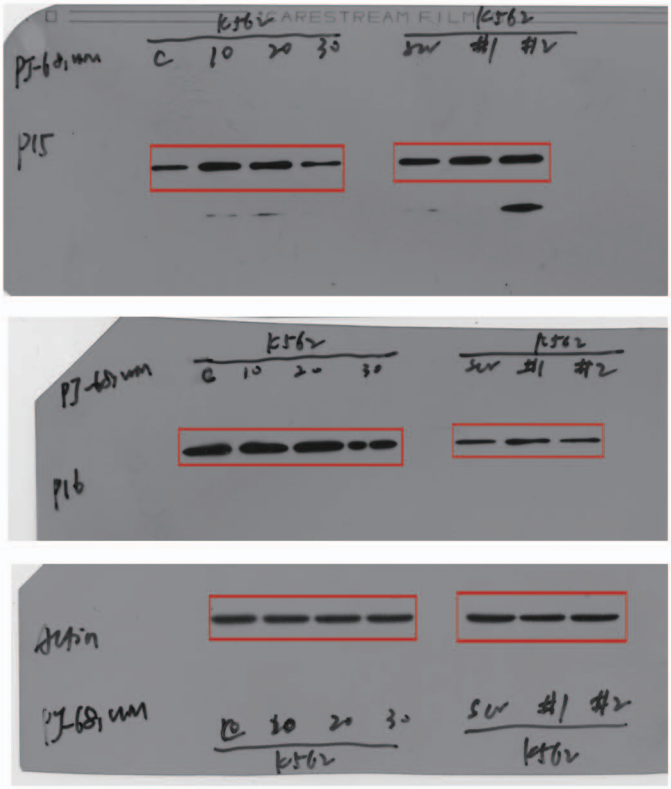

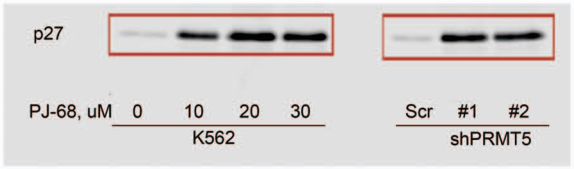

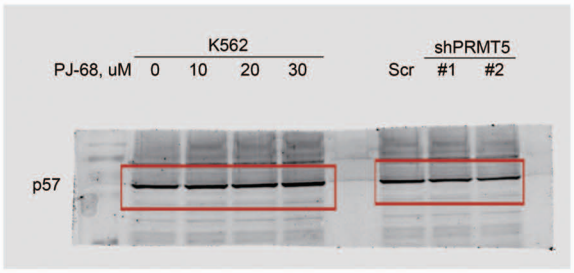

Supplemental Figure 15: Full unedited gel for Supplemental Figure 5A and 5B, red boxes indicate images shown in the corresponding Figures.

Supplemental Figure 16

Supplemental Figure 7 F

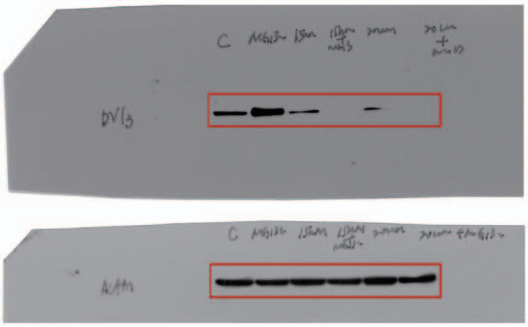

Supplemental Figure 7G

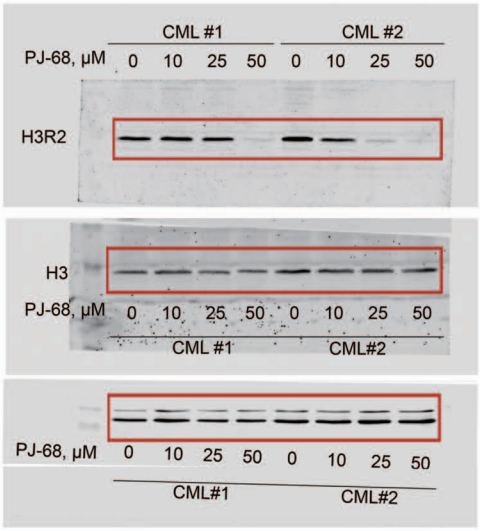

Supplemental Figure 16: Full unedited gel for Supplemental Figure 7F and 7G, red boxes indicate images shown in the corresponding Figures.